CHAPTER 98

SEDIMENT TRANSPORT AND RIPPLES DUE TO WAVES AND CURRENTS

Zbigniew PRUSZAK* and Ryszard B.ZEIDLER**

ABSTRACT

Water velocities and shear stresses have been determined for a laminar boundary layer of a progressive wave travelling over a regular series of ripples. The Lavrentiev variational method was used to transform conformally the water area with ripples into a strip with flat bottom, while the Lin approach permitted solution of the boundary layer equation.
The theoretical prediction of the bed friction was verified experimentally with a new mechanical apparatus.
By coupling the theoretical shear stress at the rippled bed with laboratory data for ripple parameters one can expose the friction conditions that control the growth and decay of ripples. If waves develop higher values of shear stress, the rippled bed becomes gradually washed out. For known shear stresses, basing on the Frijlink-Bijker formula one can compute sediment transport rates. In the respective diagram, a curve of s.t. rate versus bottom friction consists of two branches. The stages of the growth and decay of ripples are reflected in the lower and upper branches of the curve. For identical ripple height there are two values of s.t. rate , for two different wave intensities, likely to differ by as much as 25 per cent.

Three-dimensional ripples have been analyzed with regard to bed friction and compared with two-dimensional conditions.

---

* Polish Academy of Sciences' Institute of Hydro-Engineering, Gdansk, Sen. Research Scientist

** ibidem, Asst. Prof.

BOUNDARY LAYER ON RIPPLES

The dynamics of sediment and ripples depends on the characteristics of boundary layer. In order to analyze this dynamics it is reasonable to map conformally the area of motion over ripples, solve equation of motion in the basic flow region, use this solution as a background for a boundary layer equation, and determine motion inside the boundary layer. The following assumptions were made in the analysis :

1 Regular series of impermeable sinusoidal ripples preserve their form during motion
2 Ripples are exposed to regular progressive small-amplitude waves with wave height h and period T
3 Oscillatory boundary layer is laminar
4 Regular eddies are generated by waves in ripple troughs.

As shown by experiments, laminar flow at rippled bed under oscillatory motion is fairly stable. The assumption on eddies is an outcome of the studies by Sleath [6] .

A method derived by Lavrentiev [3] has been employed in our conformal mapping. The method is particularly suitable for cases with slightly different original and mapped areas of motion. Two subsequent stages of mapping, from original area with ripples, of depth H, to an elementary strip with flat bottom, are presented in Fig.1.
In the dimensionless form, the formula of mapping reads

$$w=f(z)\approx\left[\bar{x}+\frac{\eta}{2}\coth\left(\frac{2\pi H}{\lambda}\right)\sin\frac{2\pi\Delta x}{\lambda}\cosh\frac{2\pi\Delta y}{\lambda}\right]+ \qquad \ldots 1$$

$$+\,i\left[\bar{y}+\frac{\eta}{2}\coth\left(\frac{2\pi H}{\lambda}\right)\cos\left(\frac{2\pi\Delta x}{\lambda}\right)\sinh\left(\frac{2\pi\Delta y}{\lambda}\right)\right]=u(x,y)+iv(x,y)$$

in which $z = \bar{z}+\Delta z$ with the following intervals of variation

$$-\infty < \bar{x} < \infty \qquad -\eta/2 \leqslant \Delta y \leqslant \eta/2$$
$$0 < \bar{y} < H \qquad -\lambda \leqslant \Delta x \leqslant \lambda$$

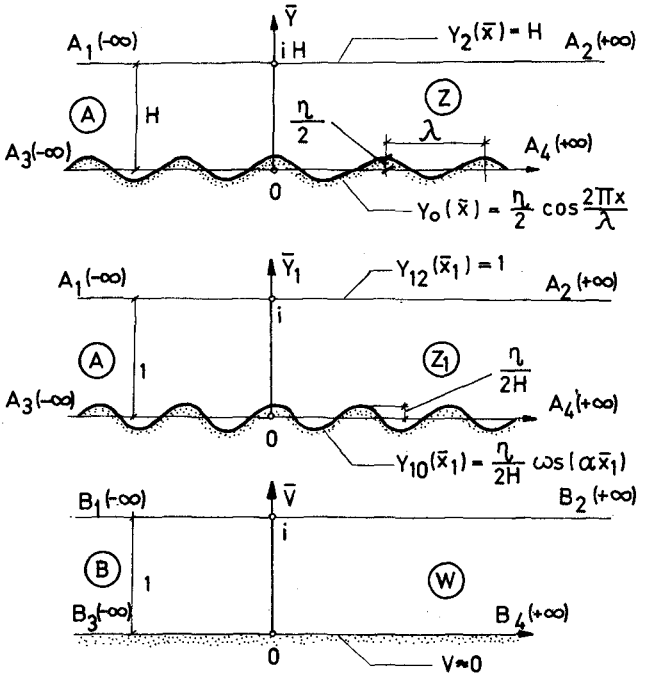

Fig.1 - Conformal Mapping

The complex velocity potential in the strip w can be chosen as

$$W(w)=\phi(u,v,t)+i\,\psi(u,v,t)=\frac{h\omega\cosh kv}{2k\sinh kH}\sin(ku-\omega t)+ \qquad \ldots 2$$

$$+\,i\,\frac{h\omega\sinh kv}{2k\sinh kH}\cos\left[ku-\omega t\right]$$

By substituting (1) in (2) and assuming $v \simeq 0$ for the lower boundary in the strip w , or $\sinh^2 kv\,(x,y) \simeq 0$, one obtains the following velocity at the upper limit of the boundary layer

$$U_1(x,y,t) = \frac{\cosh k\nu(x,y)}{\sinh kH} \cos\left[ku(x,y) - \omega t\right] \left\{1 + 2\pi \frac{\eta}{\lambda} \coth\left(\frac{2\pi H}{\lambda}\right) \times \right.$$

$$\times \cos\left(\frac{2\pi\Delta x}{\lambda}\right) \cosh\left(\frac{2\pi\Delta y}{\lambda}\right) + \pi^2 \left(\frac{\eta}{\lambda}\right)^2 \coth^2\left(\frac{2\pi H}{\lambda}\right) \cos^2\left(\frac{2\pi\Delta x}{\lambda}\right) \times \quad \ldots 3$$

$$\left. \times \cosh^2\left(\frac{2\pi\Delta y}{\lambda}\right) + \pi^2 \left(\frac{\eta}{\lambda}\right)^2 \coth^2\left(\frac{2\pi H}{\lambda}\right) \sin^2\left(\frac{2\pi\Delta x}{\lambda}\right) \sinh^2\left(\frac{2\pi\Delta y}{\lambda}\right)\right\}^{1/2}$$

One can now proceed to solution of a boundary layer equation. In 1957 Lin presented the following approximation for an unsteady laminar boundary layer:

$$\frac{\partial u}{\partial t} = \frac{\partial U}{\partial t} + \nu \frac{\partial^2 u}{\partial y^2} \qquad \ldots 4$$

The well-known boundary conditions are

$$u = 0 \text{ at } y = 0 \quad \text{and} \quad u = U \text{ at } y \to \infty \quad (\text{ or } y \to \delta\,)$$

It is possible to determine the error of the linearization inherent in Eq.4. Using Eq.3 and by comparison of the nonlinear term $U\frac{\partial U}{\partial x}$ to $\frac{\partial U}{\partial t}$ one can find the linearization errors for various values of ripple steepness. They are shown in Fig.2, for the most inaccurate situation with U_1, at the upper limit of the boundary layer.

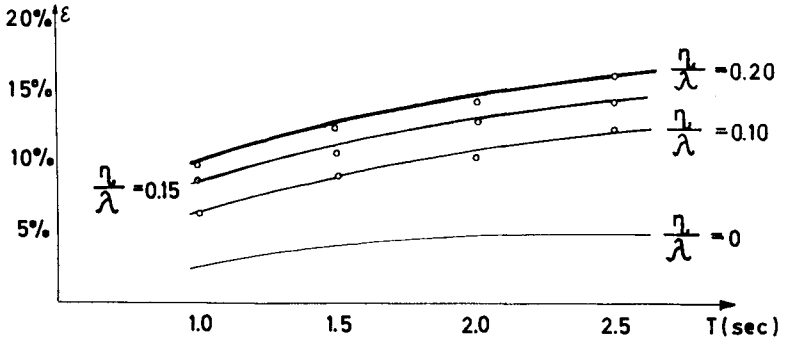

Fig.2 - Linearization Error

In general, the Lin method proves to be acceptable for fairly small bed microforms, under the studied conditions with wave periods from 1 to 2.5 (5) seconds.

The following solution [4] can be obtained from Eq.4

$$u(x,y_1,t) = u_{max}(x)\left\{\cos\left[ku(x,y)-\omega t\right] - \exp\left(-\beta y_1/X\right)\cos\left[ku(x,y)-\omega t+\beta y_1/X\right]\right\} \quad \ldots 5$$

in which

$$u_{max}(x) = \frac{h\omega}{2}\,\frac{\cosh k\nu(x,y)}{\sinh kH}\times\sqrt{1+2\pi\frac{\eta}{\lambda}\coth\left(\frac{2\pi H}{\lambda}\right)\cos\left(\frac{2\pi\Delta x}{\lambda}\right)\times \quad \ldots 6}$$

$$\times\cosh\left(\frac{2\pi\Delta y}{\lambda}\right)+\pi^2\left(\frac{\eta}{\lambda}\right)\coth^2\left(\frac{2\pi H}{\lambda}\right)\cos^2\left(\frac{2\pi\Delta x}{\lambda}\right)\cosh^2\left(\frac{2\pi\Delta y}{\lambda}\right)+$$

$$+\pi^2\left(\frac{\eta}{\lambda}\right)^2\coth^2\left(\frac{2\pi H}{\lambda}\right)\sin^2\left(\frac{2\pi\Delta x}{\lambda}\right)\sinh^2\left(\frac{2\pi\Delta y}{\lambda}\right)$$

and X is the vortex-effect parameter introduced by Sleath. By analogy, one can suggest the following formula for the bed friction

$$\tau_o^* = \frac{2\sqrt{2}\,u_{max}}{\omega h\,x_o}\cos\left[ku(x,y)-\omega t+\frac{\pi}{4}\right] \quad \ldots 7$$

in which $X_o \neq X$.

In order to determine the parameter X_o we used the data measured by Kalkanis [2]. From the comparison of this data and the results predicted by formula (7) it follows that X_o depends on $R = U_{max}\cdot\eta^2\cdot\beta\cdot\nu^{-1}$

$$X_o \simeq 0.3\,R^{0.165} \quad \ldots 8$$

An example of the computed velocity profiles is presented in Fig. 3. From analysis of the velocity fields it is clear that both velocities and their gradients above

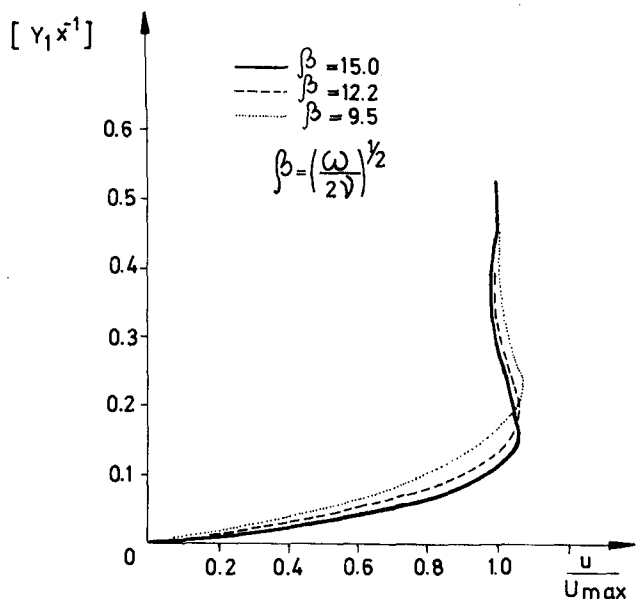

Fig.3 - Velocity Profiles in Boundary Layer

the ripple crests increase with decreasing depth of water and increasing height of water waves. The magnitudes above ripple troughs are much lower than those over the crests. The local excess of u over U, for $1.5 \leq y_1 \cdot \beta \cdot x^{-1} \leq 4.0$, is likely to be caused by the eddies generated about ripples.

The distribution of computed bed friction on ripples, both in time and space, is shown respectively in Figures 4a and 4b. In Fig.4a it can be seen that the maximum bed friction is shifted by $\omega t = \frac{\pi}{4}$ with regard to the wave crest. The values drawn in the diagram correspond to strictly defined instants, different for various points on the ripples, as if independent of the conditions in their neighborhood. On the other hand, presented in Fig.4b is the distribution generated over a certain section with ripples, as if the

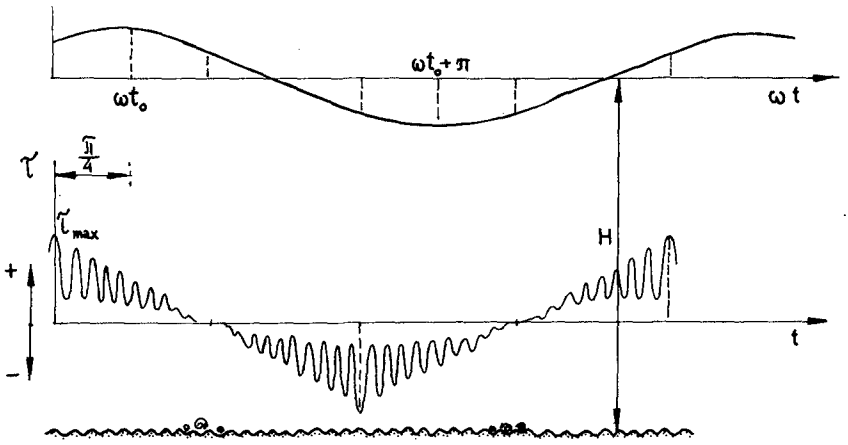

Fig.4a - Temporal Variation of Bed Friction During Consecutive Wave Phases ωt

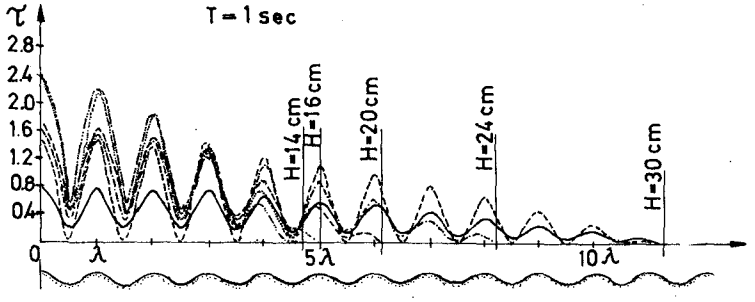

Fig.4b - Distribution of Maximum Bed Friction (for $\omega t = \frac{\pi}{4}$)

wave crest occurred at each ripple. In reality, the distributions vary in time and space, and both figures have to be combined.

EXPERIMENTAL VERIFICATION

The theoretical prediction of the bed friction on ripples was checked experimentally with a new device shown in Fig.5.

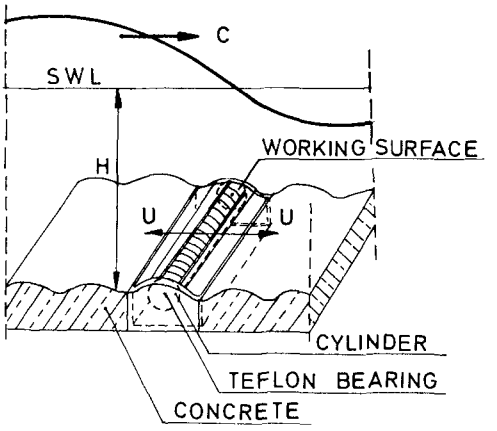

Fig.5 - Apparatus for Measurement of Bed Friction

The apparatus consists of an organic-glass cylinder, mostly sheltered in its body, the latter being flush with the crest of a ripple. The forces induced by waves are exerted in a narrow upper part of the cylinder, in the slit of the concrete ripple segment. The principle of operation consists in an angular displacement of the cylinder under the action of water. The mass of the cylinder is distributed so accurately that it moves even if minute forces are applied to its surface and returns very fast to its original position after the force is removed. Owing to a system of transverse scratches, the roughness of the exposed surface of the

cylinder is identical with that of the concrete ripples. At present, measurements of displacements of the cylinder are conducted by visual means; the calibration curve permits translation of displacements into forces. The bearing friction and the drag forces acting on the working surface of the cylinder are deducted from the total force measured with the apparatus.

The measurements of the bed friction were carried out in a wave flume with the rippled bed, a section of which is depicted in Fig.5. The waves generated in the flume had periods from 1.5 to 2.7 seconds. Because of technical difficulties, it was only a few ripple-and-wave combinations that corresponded to each other: the concrete ripple segments had forms identical with those generated by their water wave counterparts. Other pairs were incoherent, so that the results obtained for them should be treated with caution. In Table 1 they are marked with asterisks. - As can be seen from the comparison in Table 1, the computed bed friction exceeds the measured values by 10 to 40 per cent. These figures are yet smaller, below 30 percent, if one takes into account the resistance at the bearings of the measuring device. Thus, it can be claimed that the theoretical prediction of the bed friction presented in the previous section is close to reality and that the apparatus, even in its prototype version, is a promising tool in laboratory investigations.

BED FRICTION AND SEDIMENT TRANSPORT ON RIPPLES

By coupling the theoretical bed friction at rippled bed with laboratory data for ripple parameters one can expose the friction conditions that control the growth and decay of ripples. The findings for ripple height are shown in Fig.6. Four different zones, separated by three critical lines of bed friction, can be distinguished. For bed friction lower than τ_{1cr} it is only the movement of single sand grains, on a flat bed, that is possible. The zone of the generation of eddies and single ripples (whichever come first) stretches

Table 1

Bed Friction : Computed (C) Versus Measured (M)

T s	h cm	H cm	L cm	U_{max} cm/s	(C) τ_{max}	(M) τ_{max}	$\frac{\tau_{max}}{\tau_{max}}$ c/m
1.5	9.2	250	250.0	41.2	8.85	5.8	1.53*
1.5	10.5	25.0	250.0	47.1	10.12	5.8	1.74*
1.5	10.8	35.0	216.0	38.35	8.23	5.8	1.42
1.5	11.4	35.0	216.0	40.48	8.69	6.6	1.31
2.0	8.6	25.0	320.0	44.82	8.33	5.88	1.41
2.0	10.0	35.0	349.0	39.61	7.36	6.59	1.11
2.3	13.35	35.0	408.0	54.61	9.47	11.54	0.82*
2.5	11.5	25.0	388.0	58.92	9.81	8.24	1.19
2.5	11.9	35.0	445.0	49.20	8.19	8.96	0.915*
2.7	16.0	35.0	483.0	66.88	10.72	11.68	0.915*

between τ_{1cr} and τ_{2cr}, while series of ripples are formed between τ_{2cr} and τ_{3cr}. The line of τ_{3cr} marks the conditions under which the growth of ripples is completed. If waves generate higher stresses at the ripples, the latter become gradually washed out. For the sand used in our wave flume (with D_{50} = 0.025 cm and density of 2.65 gram per cubic cm) the ripples created by lower waves are unable to withstand (without irreversible deformations) shear stresses over 0.005 to 0.006 kg $cm^{-1}s^{-2}$. It can be assumed that ripples become completely destroyed if shear stresses at the bed reach 0.01 kg $cm^{-1}s^{-2}$. Under these conditions, with reconstructed flat bed, water carries suspended sediments of high concentrations.

One of the opportunities offered by the theoretical prediction of shear stresses consists in the computation

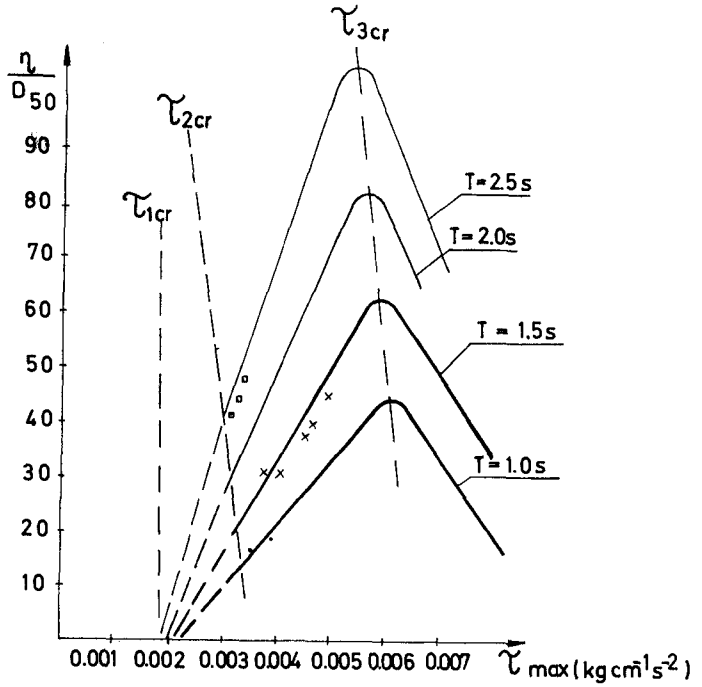

Fig.6 - Ripple Height Versus Bed Friction

of sediment transport rate, one of the most important quantities in the coastal dynamics. The computation can be based on the Frijlink formula (which is also used by Bijker [1]). Some results are presented in Fig.7 for various wave periods and velocities of longshore currents. The latter have been included in order to generalize the findings, but they are not necessary to draw the conclusions presented below. The picture illustrates general trends only, because the values of s.t. rates are local, as they were computed for the crest of the "first" ripple (where the boundary layer begins to develop). The s.t. rates averaged over the ripple length are smaller by three orders of magnitude. For comparison , analogous rates are also given for flat bed (dots for D_{50}). It should be mentioned that higher s.t. rates for rippled bed (than for flat bed) are not paradoxical: higher ripples

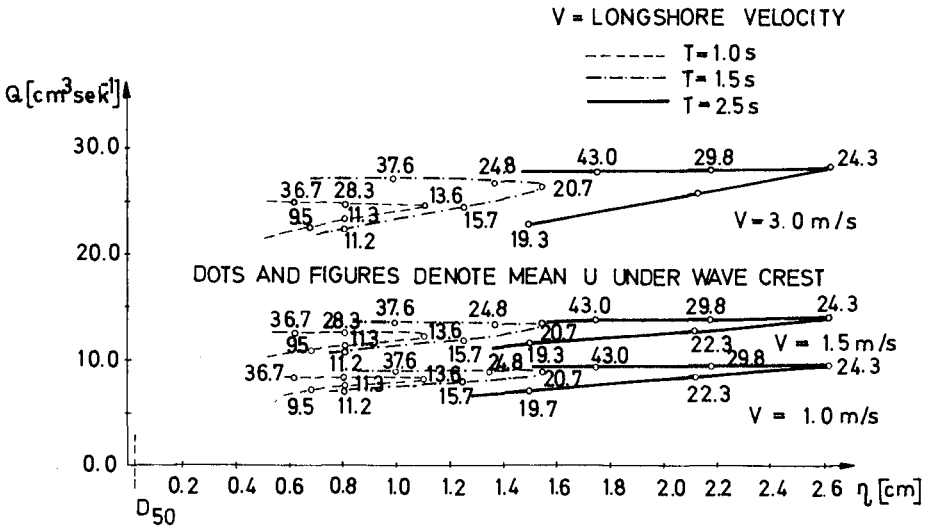

Fig.7 - Sediment Transport Rate Versus Ripple Height

bring about more resistance to motion of water but it must be remembered that, at the same time, they are produced by s t r o n g e r waves.

The stages of the growth and decay of ripples are reflected respectively in the lower and upper branches of the curves. From a similar trend observed in the wave tank it can be inferred that sediment transport sometimes differs considerably for seemingly close bed roughness conditions. For the same ripple height there occur two different values of the sediment transport rate. Depending on the strength of wave motion, which is coupled with shear stresses at the bed, a given ripple with a certain height can be in the stage of growth or washout, and the corresponding s.t.rates can differ by as much as 25 per cent.

In many existing formulas for sediment transport rates (for example, those derived by White and Ackers, Engelund and Hansen, and Bijker) the rippled bed is represented by the equivalent roughness height r . The results of this study can be used to substantiate the choice of this parameter and to revise the assumptions on r made hitherto.

THREE - DIMENSIONAL EFFECTS

Under complex conditions of coastal zones, with various systems of currents and waves and diversified configuration of beach, bed microforms are usually three-dimensional (Fig.8).

Fig.8 Three-dimensional Bed Forms in PAS-IHE Wave Tank

It is interesting to determine the origin and transformation of these forms and expose general relationships of the type $\eta, \lambda = f(\tau)$, as shown for two-dimensional forms.

Parameters of three-dimensionality can be chosen in a dozen of ways. In our analysis of the results obtained in a wave tank for two angles of wave incidence, 45° and 0 to 5°, we confined ourselves to three parameters : ripple height η, ripple length λ and the angle between ripple and local wave crest (Fig.9), Δ.

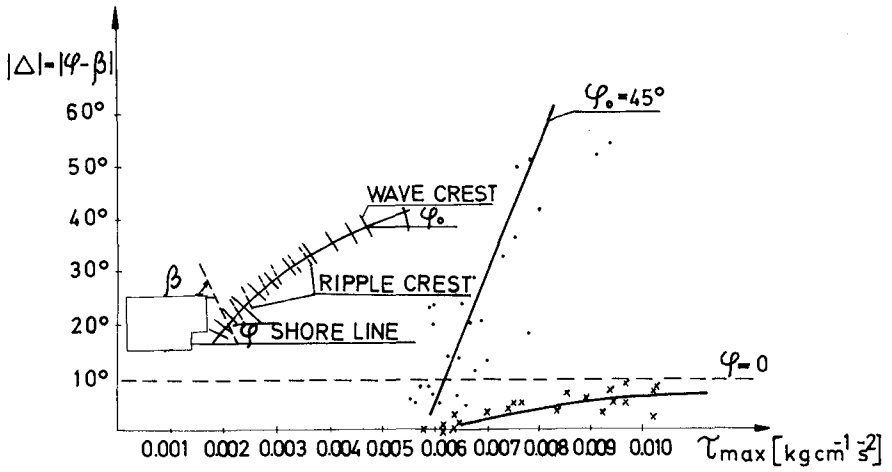

Fig.9 Ripple Misalignment Angle versus Shear Stress

The three parameters have been investigated as functions of shear stresses computed as if the ripples were two-dimensional. Thus, our definition of three-dimensionality is fairly arbitrary : 3-D conditions differ from 2-D configurations mostly by oblique layout of ripples. The angles $0 \leq \varphi \leq 5^{\circ}$ are usually linked with 2-D ripples, provided however that coastal currents are secondary (although the reverse is encountered most often).

As can be concluded from Fig.9, small angles of wave incidence (normal attack) are connected with minor misalignment of ripples, but even small changes in the layout of ripples induce considerable increase in shear stress. These situations embody local gradiental currents. For oblique incidence of waves, with more pronounced longshore currents, the misalignment

angle Δ increases much stronger as the waves aproach beach, and shear stress at the bed also increases. Both curves in Fig.9 merge at the obscisae axis about the shear stress $\tau = 0.006$ kg·cm^{-1}s^{-2}. This marks the limit at which three - -dimensional ripples begin to appear in the wave tank.

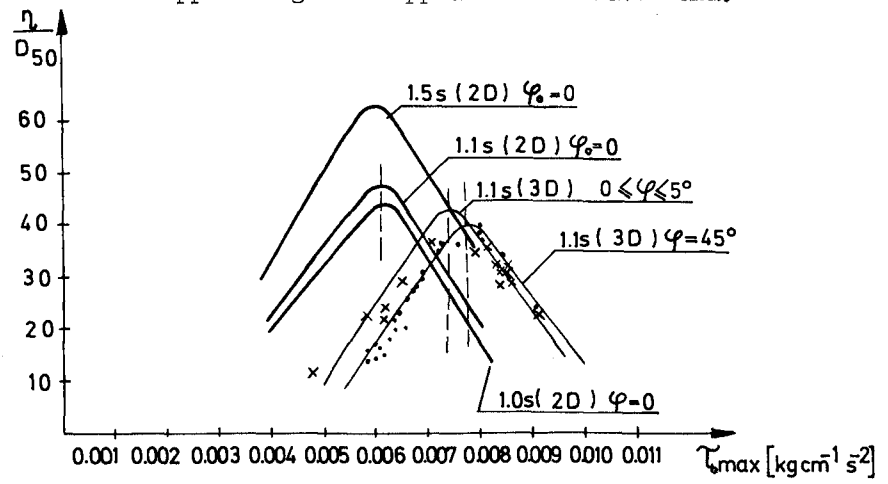

Fig.10 Height of 3-D and 2-D Ripples

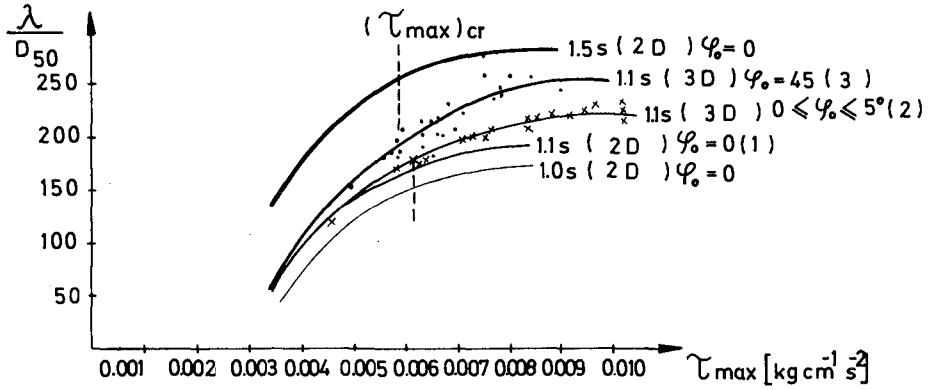

Fig.11 Length of 3-D and 2-D Ripples

Figures 10 and 11 present heights and lengths of three-dimensional ripples ; 2-D ripples are also shown for comparison. The curves suggest that the processes of the generation and decay of ripples are similar for 2-D and 3-D forms. The shift of 3-D curves, with regard to 2-D curves, is partially caused by cementing of sediments in the open-air wave tank, attacked by plankton and silt.

Three-dimensionality of bed microforms in the presence of waves and currents becomes more pronounced with higher angles of wave incidence, Ψ . Even though the shift of curve (2) with regard to (1) in Fig.10 can be attributed to cementing, the discrepencies of curves (2) and (3) are due to different Ψ . It should be noted that the scatter of the measured results around curve (3) depends on the ratio of oscillatory and longshore velocities, $U_{max} : V$. For the ratios smaller than 1 the scatter is considerable, while for $U_{max} : V > 2$ the results lie close to the curve, especially at its apex.

The three-dimensional effects in the ripple length (Fig.11) are reflected in relative increase in the length, for a given shear stress. The differences of the lengths of 2-D and 3-D ripples increase with higher shear stress. The 3-D length also increases with higher Ψ.

An important role in the generation of 3-D microforms is played by interrelations of waves and currents in the coastal zone. The effect of these factors is inherent in the angle Ψ , which determines, among others, the longshore current due to wave breaking. The variation of ripple parameters with the velocity of longshore current depends on local vectors of longshore current and wave motion. Thus, the angle Ψ determines the ripple length λ on greater depths, seawards of the breaking zone, where refraction of waves and ripples is similar, so that their directions are parallel. In the surf zone, where the effect of currents is pronounced, the three-dimensional effects become significant. Fig.12 illustrates the influence of Ψ and Δ on the increase in the length of 3-D ripples, compared to 2-D forms.

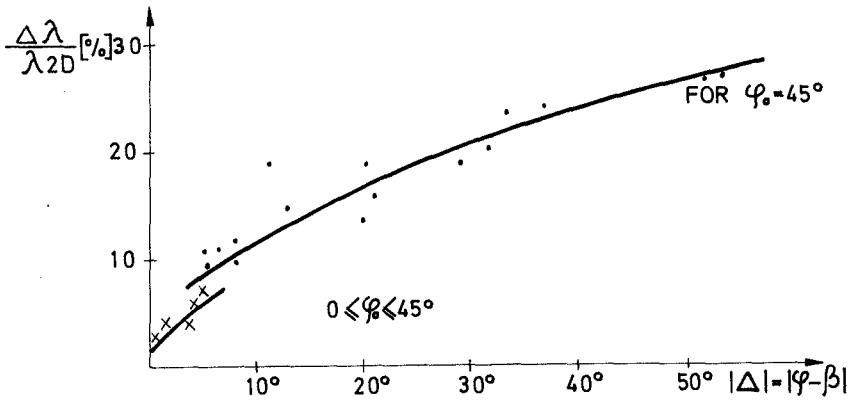

Fig.12 Relative Increase in Length of 3-D Ripples

ACKNOWLEDGEMENTS

This study has been carried out under the Polish Academy of Sciences MR I.15.3.1 programme.
The sponsorship of the Claude W.Nash Foundation, both moral and financial, is highly and sincerely appreciated.

NOTATION

h = wave height

H = depth of water

$k = \frac{2\pi}{L}$

L = wavelength

T = wave period

U_{max} = velocity at the upper limit of boundary layer, due to water wave in the crest phase

η = ripple height

λ = ripple length

ν = kinematic coefficient of viscosity

$\omega = \frac{2\pi}{T}$

REFERENCES

1 Bijker E.W., Some considerations about scales for coastal models with movable bed, Publ.No 50 Delft Hydraulics Laboratory, 1967

2 Kalkanis G., Transportation of bed material due to wave action, Technical Memorandum No 2, Beach Erosion Board, 1964

3 Lavrentiev M.A., Shabat B.W., Methods of the functions of complex variable /in Russian/, Moscow 1965

4 Pruszak Z., Processes of the formation, growth and decay of ripples in oscillatory flow /in Polish/, Rozprawy Hydrotechniczne, No 39, 1978

5 Pruszak Z., Zeidler R., Bed friction and sediment transport rate in coastal zone with bed micro-forms /in Polish/, PRACE Inst.Bud,Wodnego PAN No 4, Gdańsk 1978

6 Sleath J.F.A., A contribution to the study of vortex ripples, Journal of the Intern. Assoc.Hydr. Research, vol.13 No 3, 1975